



HHS Public Access

Author manuscript

Cell Rep. Author manuscript; available in PMC 2020 July 04.

Published in final edited form as:

Cell Rep. 2019 March 12; 26(11): 2868–2874.e3. doi:10.1016/j.celrep.2019.02.045.

Cortical State Fluctuations across Layers of V1 during Visual Spatial Perception

Anderson Speed¹, Joseph Del Rosario¹, Christopher P. Burgess², Bilal Haider^{1,3,*}

¹Biomedical Engineering, Georgia Institute of Technology and Emory University, Atlanta, GA 30332, USA

²University College London, Gower Street, London WC1E 6BT, UK

³Lead Contact

SUMMARY

Many factors modulate the state of cortical activity, but the importance of cortical state variability for sensory perception remains debated. We trained mice to detect spatially localized visual stimuli and simultaneously measured local field potentials and excitatory and inhibitory neuron populations across layers of primary visual cortex (V1). Cortical states with low spontaneous firing and correlations in excitatory neurons, and suppression of 3- to 7-Hz oscillations in layer 4, accurately predicted single-trial visual detection. Our results show that cortical states exert strong effects at the initial stage of cortical processing in V1 and can play a prominent role for visual spatial behavior in mice.

Graphical Abstract

This is an open access article under the CC BY-NC-ND license (<http://creativecommons.org/licenses/by-nc-nd/4.0/>).

*Correspondence: bilal.haider@bme.gatech.edu.

AUTHOR CONTRIBUTIONS

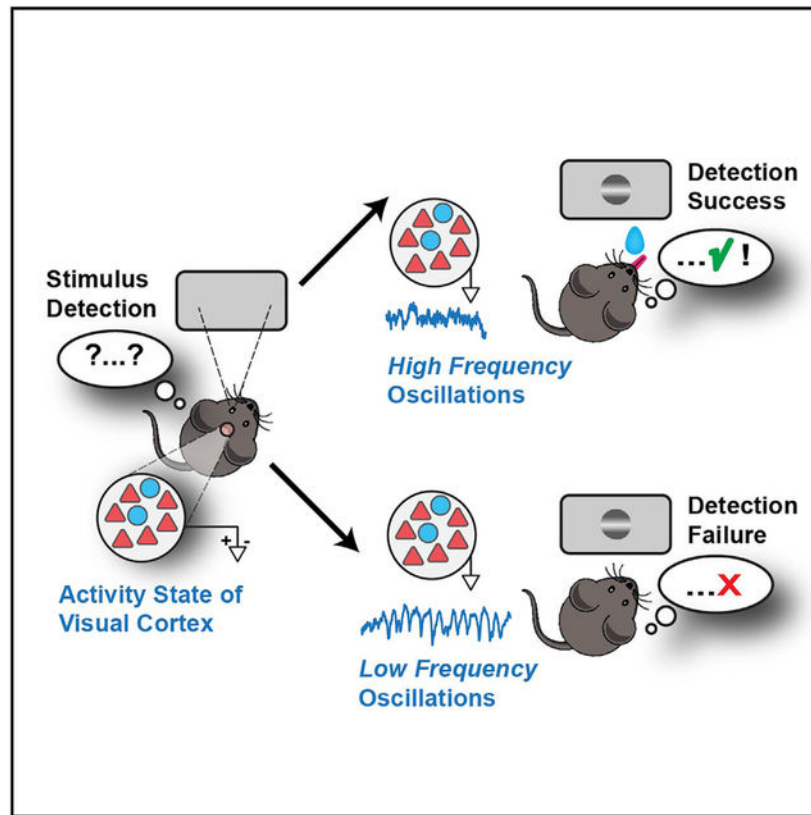
A.S., J.D.R., C.B., and B.H. performed experiments. C.B. wrote software. A.S., J.D.R., and B.H. performed analysis. B.H. and A.S. wrote the paper with input from all co-authors.

SUPPLEMENTAL INFORMATION

Supplemental Information includes can be found with this article online at <https://doi.org/10.1016/j.celrep.2019.02.045>.

DECLARATION OF INTERESTS

The authors declare no competing interests.



In Brief

Speed et al. show that visual behavior in mice is strongly influenced by the state of activity in primary visual cortex (V1). Single-trial perceptual accuracy was highly predictable from oscillations in the input layers and from correlations between excitatory neurons.

INTRODUCTION

Behavioral factors such as sleep, wakefulness, and movement have strong effects on the state of cortical activity. Cortical states are typically defined by the degree of shared fluctuations among cortical neural populations, measured by local field potential (LFP) frequency power (Harris and Thiele, 2011), and neural population correlations (Kohn et al., 2009). Cortical states exert profound effects on sensory responses (Haider and McCormick, 2009; Petersen and Crochet, 2013), but there remain unresolved questions about cortical states and their effects on sensory perception.

One question concerns the role of cortical states for perception across sensory modalities. In primates performing visual tasks, cortical states strongly influence stimulus detection (Gilbert and Li, 2013; Reynolds and Chelazzi, 2004; Spitzer et al., 1988). However, recent studies in mice show that somatosensory perception occurs in a wide variety of cortical states—even those with correlations and activity patterns resembling slow-wave sleep (Sachidhanandam et al., 2013). It is unknown how cortical states influence visual perception

in mice and unclear whether the underlying mechanisms are like those in other mammalian visual systems or like those in other mouse sensory cortical areas.

A second question concerns how cortical states coordinate excitatory and inhibitory neuron population activity during perception. In primates performing visual tasks, selective attention strongly modulates cortical state (Engel et al., 2016) and population correlations (Kohn et al., 2016; Nienborg et al., 2012). Reduction of correlated activity (decorrelation) best accounts for perceptual improvements in these tasks (Cohen and Maunsell, 2009), but the neuronal subtypes involved remain unclear. Identification of cortical neuron subtypes in higher mammals presents challenges, since action potentials of many excitatory neurons are indistinguishable from those of inhibitory neurons (Constantinople et al., 2009; Haider et al., 2010; Soares et al., 2017; Vigneswaran et al., 2011). This may hinder full understanding of excitatory and inhibitory contributions to sensory perception.

A third question concerns how cortical states affect information flow across cortical layers during sensory perception. A recent study of primate visual cortex area V4 revealed that cortical states underlying selective visual attention strongly modulate correlations in the input layers (Nandy et al., 2017). In contrast, input layers in primary visual cortex (V1) exhibit low correlations and low sensitivity to cortical state changes (Hansen et al., 2012; Poort et al., 2016; Smith et al., 2013). It remains unknown how cortical states modulate activity across input and output layers of V1 during visual perception in mice.

Several recent studies have provided insight about cortical states in awake mice. During quiet awake conditions, pupil fluctuations can index low- and high-arousal cortical states in the absence of overt behavioral changes (McGinley et al., 2015a; Reimer et al., 2014; Vinck et al., 2015). These methods have revealed how changes in neuronal correlations, LFP spectral power, and membrane potential alter sensory responsiveness. These studies suggest that there are multiple ways that key features of cortical states in awake, non-behaving conditions could impact sensory signal reliability and coding (McGinley et al., 2015b). Importantly, only one of these studies examined features of cortical states and their relationship to perception, during an auditory task (McGinley et al., 2015a). It still remains unknown how specific features of cortical states across layers of mouse V1 support visual perceptual behavior.

To address these unresolved questions, we trained mice to detect visual stimuli appearing in discrete portions of the visual field and, simultaneously, measured LFP and excitatory and inhibitory neuron populations across layers of V1. Our approach used overt behavioral outcomes as criteria to identify the features of cortical states associated with accurate visual behavior. We then quantitatively assessed how effectively each of these features predicted stimulus detection on single trials across subjects. This approach revealed that in layer 4 (L4) of V1, enhanced narrowband gamma (50–70 Hz) LFP oscillations before the stimulus and suppressed low-frequency (3–7 Hz) oscillations during the stimulus accurately predicted single-trial visual detection.

RESULTS

Visual Detection Latency and Sensitivity Depend upon Spatial Location

We designed a behavioral assay of visual spatial perception in stationary head-fixed mice (Figure 1A). Mice reported detection of visual stimuli by licking for water rewards. These were obtained only if they licked during the stimulus window (typically 1–1.5 s). Stimuli appeared only after a mandatory period of no licks had elapsed (typically 0.5–6 s, randomized per trial). Static horizontally oriented Gabor gratings appeared in one of two fixed spatial locations, either in the monocular or binocular visual fields. Gratings appeared at one of these locations for a block of 15–50 consecutive trials, and then switched to the other location for a new block of trials (Figure 1B). During training, we progressively increased task difficulty by making stimuli smaller and lower in contrast (see STAR Methods). Increasing task difficulty presented greater opportunity to examine trial-by-trial fluctuations of perception. Mice typically learned this task in 2–3 weeks and performed hundreds of trials per day.

Mice performed this detection task using vision. Stimulus location and contrast significantly affected reaction times and detection sensitivity. Mice detected binocular stimuli significantly more rapidly than monocular stimuli, even at lower contrasts (Figure 1C, left versus right panels). Moreover, within a given spatial location, higher contrast stimuli elicited significantly faster reaction times (Figure 1C). Detection sensitivity (d' ; see STAR Methods) was significantly greater than chance level in both locations, with binocular vision exhibiting greatest sensitivity (Figure 1D). Lower visual contrast decreased detection sensitivity in both locations, significantly in the binocular visual field (Figure 1D). Sensitivity to stimulus location and contrast did not depend upon grating orientation (not shown). Taken together, these results show that two major aspects of vision—spatial location and contrast—significantly influence visual detection behavior in mice. The remainder of this paper examines the neural correlates of monocular detection in the contra-lateral hemisphere.

Activity in primary visual cortex (V1) was necessary for stimulus detection. Pharmacological or optogenetic inactivation of monocular V1 abolished monocular detection, while interleaved trials of binocular detection were not significantly impaired during the same experiments (Figure S1; see STAR Methods). Inactivation of adjacent non-visual cortex caused no behavioral impairment. These results indicate that localized activity in V1 supports stimulus detection in retinotopically matched regions of visual space.

Stimulus Detection Failures Are Correlated with Strong Oscillations in L4

We performed acute recordings of laminar population activity in V1 during visual spatial detection. We recorded in monocular V1 for two reasons. First, monocular detection trials exhibited greatest task difficulty; second, monocular stimuli activate V1 unilaterally, restricting the early stimulus-evoked activity to one hemisphere. We recorded from task-relevant V1 neurons by measuring the spatial receptive field (RF) at each recording site, and ensuring that these overlapped the average location of the monocular stimuli during spatial detection (Figure S2A).

LFP was starkly different during successful versus failed detection. Detection failures (Misses) were often accompanied by synchronized, low-frequency (3–7 Hz) LFP oscillations during the stimulus (Figure 2A, gray). By functionally identifying cortical layers (Niell and Stryker, 2008; Pluta et al., 2015), we found that these 3- to 7-Hz oscillations were strongest in L4 and L5/6 (Figures S2E and S2F). Moreover, 3- to 7-Hz residual LFP power was selectively and significantly elevated only during failed detection (Miss) trials (Figures 2B–2D).

Successful detection was preceded by elevated narrowband gamma (50–70 Hz) LFP in L4. Narrowband gamma residual power was strongest in L4 (Figure S2E), and in the absence of visual contrast. Remarkably, L4 narrowband gamma power varied with behavioral outcome: it was significantly elevated and then suppressed by the onset of visual contrast selectively on Hit trials (Figures 2E–2G).

Stimulus Detection Is Correlated with Low Spontaneous Firing and Low Correlations

We next examined laminar activity of single neurons comprising two distinct classes: broad waveform regular spiking (RS) putative excitatory neurons, and narrow waveform fast-spiking (FS) putative inhibitory neurons (Figures 3A and 3B). Spike widths of FS neurons matched those of parvalbumin (PV) interneurons directly activated by channelrhodopsin (Figures S3A–S3C). This suggests that FS neurons in our experiments are PV interneurons.

RS and FS neurons displayed two distinct activations during successful detection. The initial visual response peaked and terminated rapidly, hundreds of milliseconds before the average reaction time (Hit trials; Figure 3A). By aligning to reaction times (first lick) on Hit trials, a second, rapidly rising late-phase response emerged prior to the first lick (Figure 3B); this was not present on Miss trials aligned to stimulus offset (Figure 3A, gray; see Figure S5 for Hit trial alignment to stimulus offset). Late-phase activity on Hit trials was not a movement artifact: firing terminated abruptly upon reward delivery, even though mice continued to lick vigorously during reward consumption.

Lower firing rates and reduced correlations preceded successful detection. On a cell-by-cell basis, RS and FS neurons in L2/3 and L5/6 fired significantly less before Hit versus Miss trials (Figures 3B and S3D–S3F). Accordingly, RS neuron pairs in L2/3 and L5/6 were significantly less correlated before Hit trials, as were FS pairs in L5/6 (Figure S3; correlations between Gaussian smoothed spike trains; see STAR Methods). Lower correlations prior to successful detection were not driven by higher arousal; pupil dilates with increasing arousal, yet it was significantly smaller before Hit versus Miss trials (Figure S4).

Stimuli evoked higher firing rates on Hit versus Miss trials. On a cell-by-cell basis, stimuli detected on Hit trials evoked significantly more spikes during the early sensory response in RS neurons across all layers, and in FS neurons in L4 and L2/3 (Figure 3C); this trend was even more evident after accounting for pre-stimulus activity (Figure S5). More spikes were also evoked during the late sensory response on Hit trials, particularly for FS neurons (Figure 3D; see also Figure S5).

Moreover, stimuli evoked lower noise correlations on Hit trials. RS neuron pairs in all layers displayed significantly lower noise correlations on Hit versus Miss trials, as did FS neuron pairs in L2/3 (Figure S3). These noise correlations were normally distributed across pairs, showing little evidence for discrete clusters of high and low correlation pairs (not shown).

RS Neurons and L4 LFP Oscillations Predict Single-Trial Behavior Most Accurately

Which aspects of cortical states predict trial-by-trial visual spatial detection performance? We observed robust signatures of cortical states across network, laminar, and cellular levels, even when averaging across multiple behavioral sessions and subjects. We thus quantified the accuracy of predicting single-trial behavior from cortical state signatures at both network (LFP) and cellular (RS/FS neuron) levels.

Prior to stimulus onset, RS neurons predicted single-trial behavior more accurately than FS neurons. Increased or decreased firing rates and correlations in RS neurons (associated with Hits and Misses) predicted behavioral outcomes significantly better than chance (Figure 4B; $51 \pm 4\%$ versus $56 \pm 4\%$ correctly predicted single trials; mean \pm SD; $p < 0.01$; for cross-validated SVM classifier, see STAR Methods). Firing rates and correlations of RS neurons predicted behavior better than both factors in FS neurons (see Figure S6 for laminar effects). Pre-stimulus pupil area also predicted behavioral outcomes significantly better than chance (Figure S4D; $60 \pm 3\%$).

Upon stimulus onset, L4 LFP oscillations provided the best predictions of single-trial behavior. Stimulus evoked 3- to 7-Hz L4 LFP power predicted trial outcome with $84 \pm 11\%$ accuracy, better than any other stimulus-driven factor (Figures 4C and S7). In parallel, stimulus-evoked suppression of L4 narrowband gamma LFP power predicted $71 \pm 10\%$ of single trials. A two-factor ANOVA revealed a significant interaction between time period (pre-stimulus and stimulus) and predictions from LFP power (both low-frequency and narrowband gamma power; $F = 100.5$, $p < 10^{-50}$, correction for multiple comparisons). At the level of firing rates (aggregated across layers; see STAR Methods), both RS and FS neurons predicted better than chance (RS, $55 \pm 4\%$; FS, $55 \pm 4\%$), at a level comparable to predictions from pre-stimulus rates. However, measuring stimulus-evoked firing rates relative to pre-stimulus baseline (Firing rate) significantly improved predictions (RS, $62 \pm 4\%$; FS, $63 \pm 3\%$; Figure 4D). Behavioral predictions from firing rates were particularly strong for L2/3 FS cells (Figure S6). Remarkably, pairwise noise correlations between RS neurons predicted behavioral outcome significantly better than firing rates (RS \times RS, $75 \pm 7\%$; FS \times FS, $71 \pm 4\%$; $p < 0.001$ for RS noise correlations versus RS rates). RS noise correlations were highly predictive across all layers (Figure S6). Predictions from noise correlations were not sensitive to within-trial synchrony and were not entirely explained by different numbers of spikes on Hits versus Misses (Figure S6). Finally, pupil diameter provided markedly inferior predictions of perceptual outcome compared to firing rates, noise correlations, or stimulus-evoked LFP oscillations.

DISCUSSION

Here, we revealed that specific features of cortical state fluctuations across layers of V1 play an important role for visual spatial perception in mice. Cortical states associated with lower

noise correlations, suppressed firing, and elevated gamma power before stimulus onset accurately predicted single trials of visual behavior. During the stimulus, the absence of oscillations in L4, higher stimulus-evoked firing, and lower pairwise noise correlations predicted stimulus detection. Our findings identify previously unknown neural correlates of visual perception in mice and quantify their efficacy in predicting single-trial behavior.

We revealed that multiple features of cortical states were significantly predictive of visual behavior in mice. Our study used behavioral outcome as criteria to examine features of cortical states before and during stimulus onset; we then tested how accurately these criteria predicted behavior on completely separate trials, across behavioral sessions, and across mice. We found that cortical states with high pre-stimulus firing rates and correlations predicted failures of visual detection. Recent studies of somatosensory detection found that pre-stimulus and early stimulus evoked activity in somatosensory cortex were not predictive of behavioral outcome (Sachidhanandam et al., 2013), whereas late period stimulus activity provided better behavioral predictions (Sachidhanandam et al., 2016). Differences across studies may arise from circuit organization across cortical areas, or from specific behavioral context. In our visual spatial task, monocular detection was most difficult, and this may have accentuated the relationship between cortical states and behavior (Chen et al., 2008; McGinley et al., 2015a; Spitzer et al., 1988). Compared to prior studies of full-field contrast detection (Histed et al., 2012), our task used relatively higher contrast stimuli, but these were 10-fold smaller in area (10–15° diameter circle); moreover, these stimuli were only presented to one eye in the trials considered here. Additionally, our study isolated neural correlates of cortical states and effects on perception in stationary conditions, minimizing complicated interactions between arousal, visual motion, locomotion, and motor control (Niell and Stryker, 2010; Poort et al., 2015; Saleem et al., 2013; Vaiceliunaite et al., 2013; Vinck et al., 2015). In our conditions, pupil area generally predicted behavior less accurately than the simultaneously recorded neural signatures of cortical states. Understanding the effects of cortical states on neural activity and perception across modalities, in a variety of behavioral contexts, remains an important topic for future study.

Selective coordination of population activity in specific layers of mouse V1 supported perception. First, elevated narrowband gamma power in L4 before stimulus onset was a major factor predicting correct detection, similar to the role of gamma power in visual detection in primates (Fries, 2015; Lima et al., 2011; Womelsdorf et al., 2006). Second, low levels of pre-stimulus and stimulus-evoked correlations preceded successful stimulus detection (Cohen and Maunsell, 2009; Mitchell et al., 2009). We observed that low noise correlations (decorrelation) between RS neurons predicted behavioral outcome better than firing rates, similar to studies of visual perception in primates (Cohen and Maunsell, 2009). However, FS neuron activity did not predict behavior better than RS activity, at odds with other findings (Mitchell et al., 2007; Snyder et al., 2016). This may be due to differences in RS and FS neuron identification and function in higher mammals (Constantinople et al., 2009; Soares et al., 2017; Vigneswaran et al., 2011). In mice, >90% of FS neurons are PV inhibitory neurons and >90% of RS neurons are excitatory neurons (Lee et al., 2010; Pfeffer et al., 2013; Rudy et al., 2011), enabling relatively distinct interpretation of roles of these two cell types. Our findings come with several important caveats. First, narrowband gamma in mouse V1 has origins and mechanisms distinct from broadband gamma (Saleem et al.,

2017). Second, we computed correlations on spike trains smoothed at a time-scale of the membrane time constant; the role of correlations may differ at other timescales. Finally, effects on gamma and correlations were not driven directly by visual attentional cues, a topic for further investigation.

Mouse visual behavior was most accurately predicted by cortical state features found in L4 of V1. In L4, selective modulation of narrowband gamma and suppression of 3- to 7-Hz oscillations predicted 70–80% of single behavioral trials. A recent study of L2/3 neurons described similar low-frequency oscillations, but these were also linked to changes in locomotion, and were less clearly related to behavioral outcomes (Einstein et al., 2017). We found here that these 3- to 7-Hz oscillations invaded all cortical layers but were largest and most predictive of behavior in L4. In parallel, pre-stimulus narrowband gamma was strongest in L4, and the degree of its suppression also strongly predicted behavior. Our study shows that cortical states exert widespread effects in mouse V1, and these can accurately predict perceptual outcomes on individual trials.

STAR★METHODS

CONTACT FOR REAGENT AND RESOURCE SHARING

All requests for resources should be directed to and will be fulfilled by Bilal Haider (bilal.haider@bme.gatech.edu).

EXPERIMENTAL MODEL AND SUBJECT DETAILS

All procedures were approved by the Institutional Animal Care and Use Committee at the Georgia Institute of Technology and were in agreement with guidelines established by the National Institutes of Health and the Animals (Scientific Procedures) Act 1986 (UK).

Implant surgery—Male C57BL6J mice (4–6 weeks old; reverse light cycle individual housing; bred in house; RRID: IMSR_JAX:000664) were chronically implanted with a custom-built stainless steel headplate with recording chamber (3–4 mm inner diameter) under isoflurane anesthesia (5% induction, 0.5% - 2% maintenance). The headplate was affixed to the skull using a thin layer of veterinary adhesive (VetBond) then securely bonded to the cranium (Metabond). The recording chamber was sealed with elastomer (KwikCast). Following implantation, mice were allowed to fully recover for 3 days. After recovery, animals were handled and acclimatized for 3–4 days to the head fixation apparatus, and then placed under a restricted water schedule for behavioral training. In some experiments, we performed similar procedures in male offspring of PV-cre (RRID: IMSR_JAX:017320) crossed with Ai-32-ChR2 (RRID: IMSR_JAX:024109) mice to optogenetically activate PV inhibitory neurons during behavior (Figure S1).

Water restriction—Mice learned to perform visual detection for water rewards. Mice received a minimum daily amount of water (40 ml/kg/day; 1 ml/day for a typical 25 g mouse). Reference weights were computed according to the previous methods (Burgess et al., 2017). Well-trained mice typically received all of their minimum daily water (and often more) exclusively during the task. Early in training, naive mice often received less than their

minimum amount of hydration in the task, so they received precisely measured supplemental hydration (hydrogel) to reach daily requirements.

METHOD DETAILS

Behavioral training—Mice learned the contingency between stimulus appearance and reward availability through passive instrumental conditioning. In early sessions, reward was automatically delivered after a fixed delay (0.6–0.7 s) relative to stimulus onset. With training, the latency to first lick aligned to stimulus onset occurred before reward delivery, indicating that the mouse was reacting to the visual stimulus with anticipatory licks. The mouse then transitioned to active visual detection sessions, in which reward delivery occurred only if the mouse licked during the stimulus window (typically 1.5–2 s early in training). Detection performance was quantified using the psychophysical sensitivity metric d' (Green and Swets, 1974). Hit rates were calculated from correct detection trials (licks during stimulus window) while false alarm rates were calculated from trials with blank targets (0% contrast; 20% of trials). When d' was above chance levels for 2 consecutive days, stimulus contrast range and/or size was decreased to maintain difficulty. Once animals exhibited performance above chance for both binocular and monocular stimuli of high and low contrast, we performed acute neural recordings.

Stimulus shaping—Mice detected static horizontal Gabor gratings, presented in either the binocular or monocular visual field on linearized LCD monitors (60 or 80 Hz refresh rate). Grating phase was randomized every trial, while spatial frequency (range 0.05–0.1 cycles/deg) and stimulus size (σ range 10°–20°) remained fixed across blocks of trials. Binocular contrasts ranged from 2%–75% ($38 \pm 26\%$ during recording sessions, mean \pm SD) monocular contrasts ranged from 50%–90% ($74 \pm 21\%$). During recording sessions, in addition to the detected stimuli, task-irrelevant stimuli were presented to facilitate receptive field mapping (bars 9 degrees wide, 2.5%–5% contrast, 0.1 s duration, 0.3 s interval, randomized location). These faint and brief bars did not affect behavior, and are not analyzed here.

Cortical silencing: Pharmacological: A glass micropipette (~10 μ m tip) was filled with 5 μ L of 5 μ g/ μ L muscimol (Sigma) dissolved in artificial cerebrospinal fluid. The pipette was lowered in monocular V1 to a depth of 700 μ m (L5), and positive pressure of ~17 mBar ejected 0.1 μ L over 6–10 s. The pipette was slowly withdrawn to 300 μ m, and the procedure was repeated in L2/3, as in prior studies (Komiyama et al., 2010).

Cortical silencing: Photoinhibition: In optogenetic inactivation experiments with PV-cre x Ai32(ChR2) mice (Figure S1), the skull was thinned over monocular V1 and a fiber-coupled LED (473 nm) delivered pulses of light to inactivate V1 on 25% of detection trials (1 s during visual stimulus, starting 0.1 s before stimulus and ramping to 5.8 mW measured at the cranium).

Recordings: Surgical preparation: On the day of recording, mice were anesthetized with isoflurane and a small (~100–500 μ m) craniotomy was opened over the monocular portion

of V1 (0.5 mm anterior to lambda, 2–2.5 mm lateral to central suture). Mice recovered for at least 3 hours prior to recording during behavior.

Recordings: Electrophysiology: Recordings were done with multi-site silicon probes (NeuroNexus) consisting of either a single 32-channel shank, or two 16-channel shanks. Electrodes were advanced ~1000 μm below the cortical surface. Data were collected for the duration of a behavioral session (typically 100–300 trials), after which a task-irrelevant stimulus was presented to facilitate receptive field mapping of the recording site (100% contrast vertical flashed bars, 9 degrees in width, duration 0.1 s, inter-stimulus interval 0.3 s, placed in random locations tiling 144 degrees of the visual field). The craniotomy was kept sterile and covered with silicone elastomer in between consecutive recording days (typically 2–4 from the same site).

Recordings: Eye Tracking: In a subset of mice, we simultaneously recorded the pupil (6 mice across 59 sessions and 3476 trials). A high speed camera (Imaging source DMK 21Bu04.H) with a zoom lens (Navitar 7000) and infrared filter (Mightex, 092/52 \times 0.75) was placed approximately 22 cm from the animal's right eye under near-infrared LED illumination (Mightex, SLS-02008-A). Video files were acquired and processed using the Image Acquisition Toolbox in MATLAB. 1 mm corresponded to ~74 pixels on each frame.

Data analysis: Spike sorting: Raw electrical signals were amplified and digitized (Blackrock Microsystems) then exported for post processing. Extracellular spikes were isolated using the KlustaViewa Suite (Rossant et al., 2016). Briefly, automated clustering was followed by three manual steps. First, obvious noise artifacts were eliminated. Second, poorly isolated waveforms were classified as multiunit activity. Waveforms of the remaining clusters were carefully curated in PCA space in parallel with unit auto- and cross-correlation histograms to define well-isolated single units. A small number of units ($n = 7$) with low signal to noise ratio (SNR) < 3 were excluded because of unreliable measurement of spike widths. No additional criteria were used to include or exclude units from further analysis. The average SNR of our units ($n = 224$) was 35.0, and the average recording yield was 17.2 ± 8.9 units per session (mean \pm SD).

We classified Fast spiking (FS) and Regular Spiking (RS) units according to spike width. Histograms of population spike widths (measured peak to trough) were clearly bimodal (Figure S3). Units with a peak-to-trough width less than 0.57 ms were classified as FS, and broader units classified as RS. This classification of FS neurons closely agrees with previous studies of mouse V1 (Niell and Stryker, 2010), where FS neurons consist nearly exclusively of parvalbumin (PV) positive inhibitory neurons (Pfeffer et al., 2013). We additionally verified the inhibitory identity of FS neurons in our awake recording conditions by expressing channelrhodopsin in parvalbumin (PV) interneurons, and measuring spikes of PV interneurons directly activated by light (Figure S3).

Data analysis: Correlations: Spike trains were convolved with a Gaussian filter (half-width 10 ms), and cross correlations were calculated between smoothed spike trains on a trial-by-trial basis (MATLAB `xcorr` function with 'coeff' normalization). This normalization scales the cross correlation by the maximum value of the autocorrelation. For all correlation

analyses, we used the peak value of the cross correlation across all lags. Pre-stimulus period correlations were calculated during blank (gray screen) conditions and limited to a maximum of 3 s (or less, if the inter-trial interval was smaller on that particular trial, range: 0.5 – 3 s). Noise correlations were calculated trial-by-trial by subtracting the mean stimulus response (per neuron, averaged across all trials) from the individual spike trains on those particular trials (Schulz et al., 2015). Cross correlations were then calculated as described above. This measure of residual spike train correlation during the stimulus is related to but distinct from other measures of noise correlations (e.g., spike count correlations; Cohen and Kohn, 2011). Stimulus period spike trains consisted of the 0.5 s preceding the stimulus onset until the reaction time for correct trials, or until stimulus offset (1 – 2 s) for failed detection trials.

Data analysis: Classifier: We trained a support vector machine (SVM) classifier to predict behavioral outcome from simultaneously recorded neural activity (1175 hit trials, 1031 miss trials). Training sets consisted of firing rates or correlations sub-sampled in a ratio and sum that matched the average recording session (~5 FS cells and ~15 RS cells). For layer specific correlations, we sub-sampled a total of 15 neuron pairs within specific layers per trial, again to match statistics of the average recording session. Training and testing sets consisted of 200 trials each (100 hit and 100 miss). Classifier performance was determined by the fraction of correctly classified trials in the testing set (MATLAB ‘fitsvm’ function). Gaussian kernels for SVM classification were optimized using a bayesian optimization procedure (MATLAB ‘bayesopt’ function). This entire procedure was repeated 50 times to compute the mean and standard deviation of classifier performance for the dataset.

In a similar way, we constructed a classifier with the time series of pupil diameter in the 3 s preceding the stimulus. Again, training and testing sets consisted of 100 randomly selected hit and miss trials, and performance was determined by fraction of correctly classified trials in the testing set.

Trial classification with LFP gamma power used the residual power spectrum of the LFP between 50–70Hz, and low frequency LFP power 5 – 10 Hz, with the same training and testing parameters described above.

Data analysis: Pupil: We first sub-selected a region of interest that captured changes in pupil for all frames in the file (Figure S4A). Frames were then smoothed using a 2D Gaussian filter. We then selected intensities to separate the pixels within and outside of the pupil. A contour was drawn according to the identified intensities, and a least-squares error 2D ellipse was fit to the contours. Pupil area was calculated as the percent deviation from the mean $[(A - \bar{A}) * 100 / \bar{A}]$, where A is the area in pixels and \bar{A} is the average area across all frames. If an ellipse could not be fit, a NaN value was inserted for that frame. For analysis of pupil position, we looked at changes in the azimuthal coordinate of the fitted ellipse across frames, since this was the axis in which stimulus position varied.

Data analysis: LFP: Local field potentials were obtained by bandpass filtering raw neural signals from 0.3 to 200 Hz. Laminar LFP responses were calculated by using current source density analysis (Figure S2), and averaging across channels within an identified layer. We

defined L4 to span ± 100 microns around the location of the earliest and largest CSD sink, consistent with prior functional and anatomical localization of L4 in mouse V1 (Lien and Scanziani, 2013; Pluta et al., 2015). We then averaged laminar LFP responses across behavioral sessions and animals (11 mice, 15 sessions, 2206 trials) to evaluate differences for Hit and Miss trials.

We analyzed the excess (residual) LFP power during Hit and Miss trials in low (2–20 Hz) and narrowband gamma (50–70 Hz) frequencies. As in our previous studies, we calculated residual power by fitting the entire power spectrum with a single exponential that excluded the band of interest. The difference (actual – fit) is divided by the fit to obtain fractional residual power. The power spectral density (fast Fourier transform (FFT) of the autocorrelation of the LFP) was calculated during the pre-stimulus and stimulus presentation epochs. Narrowband gamma (50–70 Hz) residual power was estimated by fitting the spectral density between 30–90 Hz, excluding 50–70 (Saleem et al., 2017). Residual low frequency power was estimated in the same manner, by fitting between 2–20 Hz excluding 4–12 Hz. Residual power was calculated per trial.

QUANTIFICATION AND STATISTICAL ANALYSIS

The total neural dataset consisted of 15 recording sessions from 11 mice, 1175 hit trials, 1031 miss trials, $n = 224$ units (52 FS cells, 172 RS cells). All details of statistical comparisons and definition of center and dispersion are contained in the figure legends. In general, non-parametric Wilcoxon rank sum tests (unpaired data), signed rank tests (paired data), or Kruskal-Wallis ANOVA tests (corrected for multiple comparisons) were performed, unless otherwise noted. Significance was defined at $\alpha = 0.05$, unless noted. No strategies were employed for randomization of subjects, recordings, data collection, or analysis. Aside from spike sorting quality metrics, no neural data was excluded from analysis. Algorithmic strategies for randomization and error estimation (e.g., classifier cross-validation) are described in the relevant sections. No tests were used to justify sample size, but ours is comparable to several recent studies of behaving mice (Poort et al., 2015; Saleem et al., 2017; Vaiceliunaite et al., 2013; Vinck et al., 2015).

DATA AND SOFTWARE AVAILABILITY

Data structures and MATLAB code necessary for reproducing results of the manuscript are available from the lead contact upon reasonable request.

Supplementary Material

Refer to Web version on PubMed Central for supplementary material.

ACKNOWLEDGMENTS

We thank Aman Saleem for critical comments on an earlier version of this work; Tatsuo Sato, Michael Krumin, Charu Reddy, Alexander Zorn, and Hayley Arrowood for technical assistance; and Matteo Carandini for generous support in the initial phase of this study (Wellcome Trust Grants 095668 and 095669). J.D.R. was funded by a Goizueta Foundation Fellowship. B.H. was funded by the National Science Foundation IRFP, GT Neural Engineering Center, Whitehall Foundation, Sloan Foundation, and National Institute of Neurological Disorders and Stroke (NIH 1R01 NS107968).

REFERENCES

- Burgess CP, Lak A, Steinmetz NA, Zátka-Haas P, Bai Reddy C, Jacobs EAK, Linden JF, Paton JJ, Ranson A, Schröder S, et al. (2017). High-yield methods for accurate two-alternative visual psychophysics in head-fixed mice. *Cell Rep.* 20, 2513–2524. [PubMed: 28877482]
- Chen Y, Martinez-Conde S, Macknik SL, Bereshpolova Y, Swadlow HA, and Alonso JM (2008). Task difficulty modulates the activity of specific neuronal populations in primary visual cortex. *Nat. Neurosci* 11, 974–982. [PubMed: 18604204]
- Cohen MR, and Kohn A (2011). Measuring and interpreting neuronal correlations. *Nat. Neurosci* 14, 811–819. [PubMed: 21709677]
- Cohen MR, and Maunsell JH (2009). Attention improves performance primarily by reducing interneuronal correlations. *Nat. Neurosci* 12, 1594–1600. [PubMed: 19915566]
- Constantinople CM, Disney AA, Maffie J, Rudy B, and Hawken MJ (2009). Quantitative analysis of neurons with Kv3 potassium channel subunits, Kv3.1b and Kv3.2, in macaque primary visual cortex. *J. Comp. Neurol* 516, 291–311. [PubMed: 19634181]
- Einstein MC, Polack PO, Tran DT, and Golshani P (2017). Visually evoked 3–5 Hz membrane potential oscillations reduce the responsiveness of visual cortex neurons in awake behaving mice. *J. Neurosci* 37, 5084–5098. [PubMed: 28432140]
- Engel TA, Steinmetz NA, Gieselmann MA, Thiele A, Moore T, and Boahen K (2016). Selective modulation of cortical state during spatial attention. *Science* 354, 1140–1144. [PubMed: 27934763]
- Fries P (2015). Rhythms for cognition: communication through coherence. *Neuron* 88, 220–235. [PubMed: 26447583]
- Gilbert CD, and Li W (2013). Top-down influences on visual processing. *Nat. Rev. Neurosci* 14, 350–363. [PubMed: 23595013]
- Green DM, and Swets JA (1974). *Signal Detection Theory and Psychophysics* (R. E. Krieger Publishing Company).
- Haider B, and McCormick DA (2009). Rapid neocortical dynamics: cellular and network mechanisms. *Neuron* 62, 171–189. [PubMed: 19409263]
- Haider B, Krause MR, Duque A, Yu Y, Touryan J, Mazer JA, and McCormick DA (2010). Synaptic and network mechanisms of sparse and reliable visual cortical activity during nonclassical receptive field stimulation. *Neuron* 65, 107–121. [PubMed: 20152117]
- Hansen BJ, Chelaru MI, and Dragoi V (2012). Correlated variability in laminar cortical circuits. *Neuron* 76, 590–602. [PubMed: 23141070]
- Harris KD, and Thiele A (2011). Cortical state and attention. *Nat. Rev. Neurosci* 12, 509–523. [PubMed: 21829219]
- Histed MH, Carvalho LA, and Maunsell JH (2012). Psychophysical measurement of contrast sensitivity in the behaving mouse. *J. Neurophysiol* 107, 758–765. [PubMed: 22049334]
- Kohn A, Zandvakili A, and Smith MA (2009). Correlations and brain states: from electrophysiology to functional imaging. *Curr. Opin. Neurobiol* 19, 434–438. [PubMed: 19608406]
- Kohn A, Coen-Cagli R, Kanitscheider I, and Pouget A (2016). Correlations and neuronal population information. *Annu. Rev. Neurosci* 39, 237–256. [PubMed: 27145916]
- Komiyama T, Sato TR, O'Connor DH, Zhang YX, Huber D, Hooks BM, Gabitto M, and Svoboda K (2010). Learning-related fine-scale specificity imaged in motor cortex circuits of behaving mice. *Nature* 464, 1182–1186. [PubMed: 20376005]
- Lee S, Hjerling-Leffler J, Zaghera E, Fishell G, and Rudy B (2010). The largest group of superficial neocortical GABAergic interneurons expresses ionotropic serotonin receptors. *J. Neurosci* 30, 16796–16808. [PubMed: 21159951]
- Lien AD, and Scanziani M (2013). Tuned thalamic excitation is amplified by visual cortical circuits. *Nat. Neurosci* 16, 1315–1323. [PubMed: 23933748]
- Lima B, Singer W, and Neuenschwander S (2011). Gamma responses correlate with temporal expectation in monkey primary visual cortex. *J. Neurosci* 31, 15919–15931. [PubMed: 22049435]
- McGinley MJ, David SV, and McCormick DA (2015a). Cortical membrane potential signature of optimal states for sensory signal detection. *Neuron* 87, 179–192. [PubMed: 26074005]

- McGinley MJ, Vinck M, Reimer J, Batista-Brito R, Zaghera E, Cadwell CR, Tolias AS, Cardin JA, and McCormick DA (2015b). Waking state: rapid variations modulate neural and behavioral responses. *Neuron* 87, 1143–1161. [PubMed: 26402600]
- Mitchell JF, Sundberg KA, and Reynolds JH (2007). Differential attention-dependent response modulation across cell classes in macaque visual area V4. *Neuron* 55, 131–141. [PubMed: 17610822]
- Mitchell JF, Sundberg KA, and Reynolds JH (2009). Spatial attention decorrelates intrinsic activity fluctuations in macaque area V4. *Neuron* 63, 879–888. [PubMed: 19778515]
- Nandy AS, Nassi JJ, and Reynolds JH (2017). Laminar organization of attentional modulation in macaque visual area V4. *Neuron* 93, 235–246. [PubMed: 27989456]
- Niell CM, and Stryker MP (2008). Highly selective receptive fields in mouse visual cortex. *J. Neurosci* 28, 7520–7536. [PubMed: 18650330]
- Niell CM, and Stryker MP (2010). Modulation of visual responses by behavioral state in mouse visual cortex. *Neuron* 65, 472–479. [PubMed: 20188652]
- Nienborg H, Cohen MR, and Cumming BG (2012). Decision-related activity in sensory neurons: correlations among neurons and with behavior. *Annu. Rev. Neurosci* 35, 463–483. [PubMed: 22483043]
- Petersen CC, and Crochet S (2013). Synaptic computation and sensory processing in neocortical layer 2/3. *Neuron* 78, 28–48. [PubMed: 23583106]
- Pfeffer CK, Xue M, He M, Huang ZJ, and Scanziani M (2013). Inhibition of inhibition in visual cortex: the logic of connections between molecularly distinct interneurons. *Nat. Neurosci* 16, 1068–1076. [PubMed: 23817549]
- Pluta S, Naka A, Veit J, Telian G, Yao L, Hakim R, Taylor D, and Adesnik H (2015). A direct translaminar inhibitory circuit tunes cortical output. *Nat. Neurosci* 18, 1631–1640. [PubMed: 26414615]
- Poort J, Khan AG, Pachitariu M, Nemri A, Orsolich I, Krupic J, Bauza M, Sahani M, Keller GB, Mrsic-Flogel TD, and Hofer SB (2015). Learning enhances sensory and multiple non-sensory representations in primary visual cortex. *Neuron* 86, 1478–1490. [PubMed: 26051421]
- Poort J, Self MW, van Vugt B, Malkki H, and Roelfsema PR (2016). Texture segregation causes early figure enhancement and later ground suppression in areas V1 and V4 of visual cortex. *Cereb. Cortex* 26, 3964–3976. [PubMed: 27522074]
- Reimer J, Froudarakis E, Cadwell CR, Yatsenko D, Denfield GH, and Tolias AS (2014). Pupil fluctuations track fast switching of cortical states during quiet wakefulness. *Neuron* 84, 355–362. [PubMed: 25374359]
- Reynolds JH, and Chelazzi L (2004). Attentional modulation of visual processing. *Annu. Rev. Neurosci* 27, 611–647. [PubMed: 15217345]
- Rossant C, Kadir SN, Goodman DFM, Schulman J, Hunter MLD, Saleem AB, Grosmark A, Belluscio M, Denfield GH, Ecker AS, et al. (2016). Spike sorting for large, dense electrode arrays. *Nat. Neurosci* 19, 634–641. [PubMed: 26974951]
- Rudy B, Fishell G, Lee S, and Hjerling-Leffler J (2011). Three groups of interneurons account for nearly 100% of neocortical GABAergic neurons. *Dev. Neurobiol* 71, 45–61. [PubMed: 21154909]
- Sachidhanandam S, Sreenivasan V, Kyriakatos A, Kremer Y, and Petersen CC (2013). Membrane potential correlates of sensory perception in mouse barrel cortex. *Nat. Neurosci* 16, 1671–1677. [PubMed: 24097038]
- Sachidhanandam S, Sermet BS, and Petersen CCH (2016). Parvalbumin-expressing GABAergic neurons in mouse barrel cortex contribute to gating a goal-directed sensorimotor transformation. *Cell Rep.* 15, 700–706. [PubMed: 27149853]
- Saleem AB, Ayaz A, Jeffery KJ, Harris KD, and Carandini M (2013). Integration of visual motion and locomotion in mouse visual cortex. *Nat. Neurosci* 16, 1864–1869. [PubMed: 24185423]
- Saleem AB, Lien AD, Krumin M, Haider B, Rosón MR, Ayaz A, Reinhold K, Busse L, Carandini M, and Harris KD (2017). Subcortical source and modulation of the narrowband gamma oscillation in mouse visual cortex. *Neuron* 93, 315–322. [PubMed: 28103479]
- Schulz DP, Sahani M, and Carandini M (2015). Five key factors determining pairwise correlations in visual cortex. *J. Neurophysiol* 114, 1022–1033. [PubMed: 26019310]

- Smith MA, Jia X, Zandvakili A, and Kohn A (2013). Laminar dependence of neuronal correlations in visual cortex. *J. Neurophysiol* 109, 940–947. [PubMed: 23197461]
- Snyder AC, Morais MJ, and Smith MA (2016). Dynamics of excitatory and inhibitory networks are differentially altered by selective attention. *J. Neurophysiol* 116, 1807–1820. [PubMed: 27466133]
- Soares D, Goldrick I, Lemon RN, Kraskov A, Greensmith L, and Kalmar B (2017). Expression of Kv3.1b potassium channel is widespread in macaque motor cortex pyramidal cells: a histological comparison between rat and macaque. *J. Comp. Neurol* 525, 2164–2174. [PubMed: 28213922]
- Spitzer H, Desimone R, and Moran J (1988). Increased attention enhances both behavioral and neuronal performance. *Science* 240, 338–340. [PubMed: 3353728]
- Vaiceleunaite A, Eriskien S, Franzen F, Katzner S, and Busse L (2013). Spatial integration in mouse primary visual cortex. *J. Neurophysiol* 110, 964–972. [PubMed: 23719206]
- Vigneswaran G, Kraskov A, and Lemon RN (2011). Large identified pyramidal cells in macaque motor and premotor cortex exhibit “thin spikes”: implications for cell type classification. *J. Neurosci* 31, 14235–14242. [PubMed: 21976508]
- Vinck M, Batista-Brito R, Knoblich U, and Cardin JA (2015). Arousal and locomotion make distinct contributions to cortical activity patterns and visual encoding. *Neuron* 86, 740–754. [PubMed: 25892300]
- Womelsdorf T, Fries P, Mitra PP, and Desimone R (2006). Gamma-band synchronization in visual cortex predicts speed of change detection. *Nature* 439, 733–736. [PubMed: 16372022]

Highlights

- The state of activity in primary visual cortex (V1) influences perception in mice.
- Low-frequency oscillations in layer 4 hinder stimulus detection.
- Narrowband gamma oscillations in layer 4 promote stimulus detection.
- These two key aspects of cortical states accurately predict single-trial behavior.

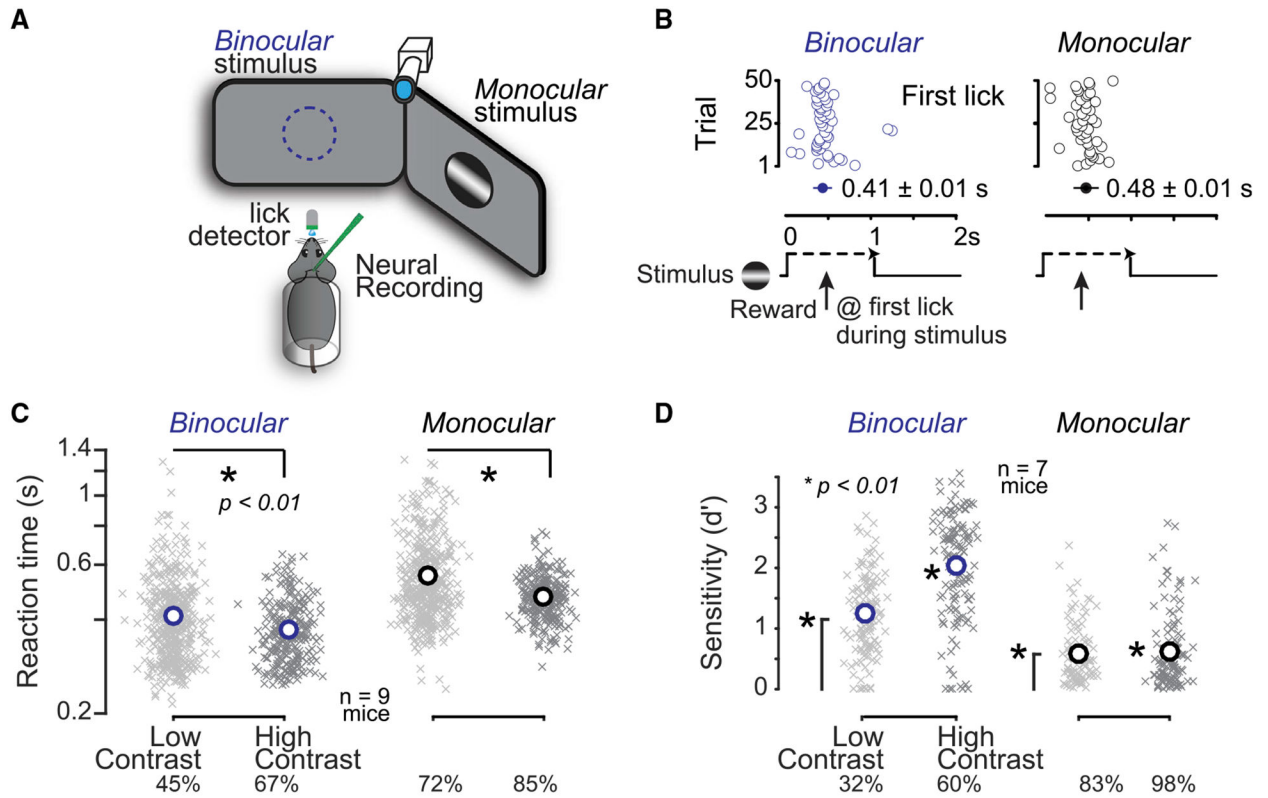


Figure 1. Visual Detection Latency and Sensitivity Depend upon Spatial Location

(A) Head-fixed mice faced two monitors placed in the binocular (blue) and monocular (black) visual fields. Mice reported detection of visual stimuli (gratings) by licking for water. A photosensor recorded licks, a camera monitored the right eye, and silicon probes recorded activity in the left hemisphere. (B) Example session of visual detection, where stimuli appeared in one location for 50 consecutive trials, and then switched to the other location for 50 trials. Mice obtained reward upon first lick (open circles) during the stimulus presentation window (1-s duration). Reaction times were faster for binocular (blue) versus monocular detection (black). (C) Reaction times decreased with increased stimulus contrast. Crosses indicate mean reaction time per block of 10–50 trials, circles indicate population mean reaction time ($n = 9$ mice, 752 blocks, >30k trials; last quartile of total training sessions). Binocular (blue): low contrast, 0.41 ± 0.04 s; high contrast, 0.37 ± 0.03 ; mean \pm SEM; $p < 0.01$ rank sum test. Monocular (black): low contrast, 0.56 ± 0.06 s; high contrast, 0.47 ± 0.03 ; mean \pm SEM; $p < 0.01$ rank sum test. Binocular low and high contrasts (mean), 45% and 67%; monocular low and high contrasts (mean), 72% and 85%. (D) Detection sensitivity (d') improved with higher stimulus contrast. Crosses indicate d' per daily session ($n = 7$ mice, 475 sessions, >115k trials from last quartile of training days). Circles indicate population mean. Binocular (blue): low contrast, 1.25 ± 0.06 ; high contrast, 2.04 ± 0.08 ; mean \pm SEM; monocular (black): low contrast, 0.59 ± 0.05 ; high contrast, 0.62 ± 0.06 ; mean \pm SEM. All population means significantly greater than chance level ($p < 0.01$, sign test). Binocular sensitivity varied significantly with contrast ($p < 0.01$, rank sum test). Monocular sensitivity not different with contrast ($p = 0.4$). Binocular contrast means: 32% and 60%;

monocular contrast means: 83% and 98%. Behavioral performance required V1 activity (Figure S1).

Author Manuscript

Author Manuscript

Author Manuscript

Author Manuscript

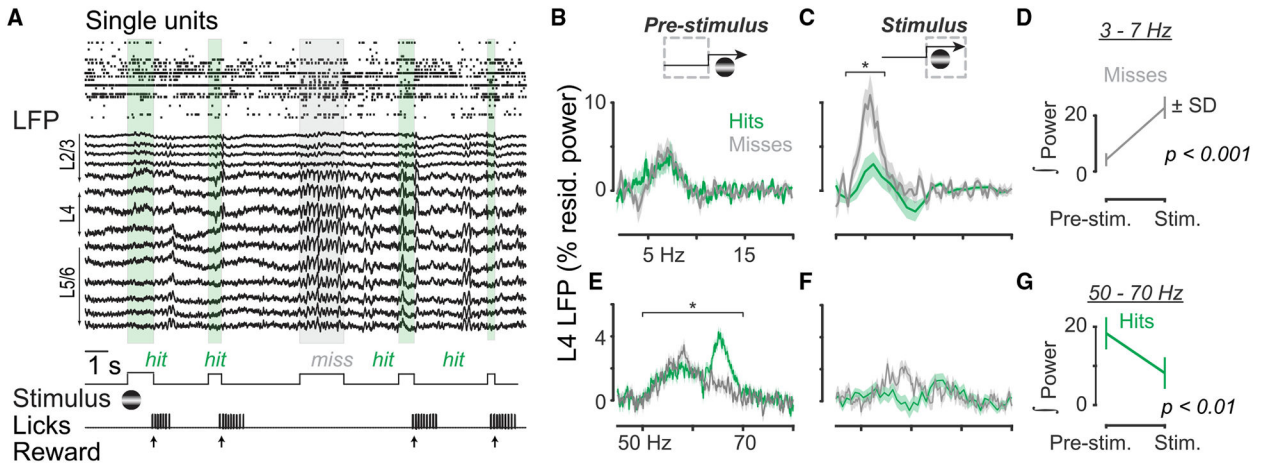


Figure 2. Cortical State Signatures in Layer 4 LFP during Visual Spatial Detection

(A) Single units and local field potential (LFP) recorded simultaneously with a multisite probe in monocular visual cortex (V1) during visual detection. Layers 2/3 (L2/3), L4, and L5/6 estimated by current source density analysis (see Figure S2). Detection failure (Miss; gray box) occurred in the midst of successful detection trials (Hits; green boxes). (B and C) L4 LFP residual power in 2- to 20-Hz range on Hit (green) and Miss (gray) trials, measured for the pre-stimulus (B) and stimulus (C) periods. Traces indicate mean \pm SEM; $n = 15$ sessions in 11 mice. Residual power integrated from 3 to 7 Hz significantly greater on Miss versus Hit trials during stimulus (paired signed rank test, $p < 0.01$). No significant difference between Hits and Misses pre-stimulus ($p > 0.4$). (D) Significantly elevated 3- to 7-Hz integrated power on Miss trials during stimulus (paired signed rank test, $p < 0.01$). (E and F) L4 LFP residual narrowband gamma (50–70 Hz) power on Hit (green) and Miss (gray) trials, measured for the pre-stimulus (E) and stimulus (F) periods. Residual power integrated from 50 to 70 Hz significantly greater on Hit versus Miss trials before stimulus (paired signed rank test, $p < 0.01$). (G) Significantly reduced 50- to 70-Hz integrated power on Hit trials during stimulus (paired signed rank test, $p < 0.01$).

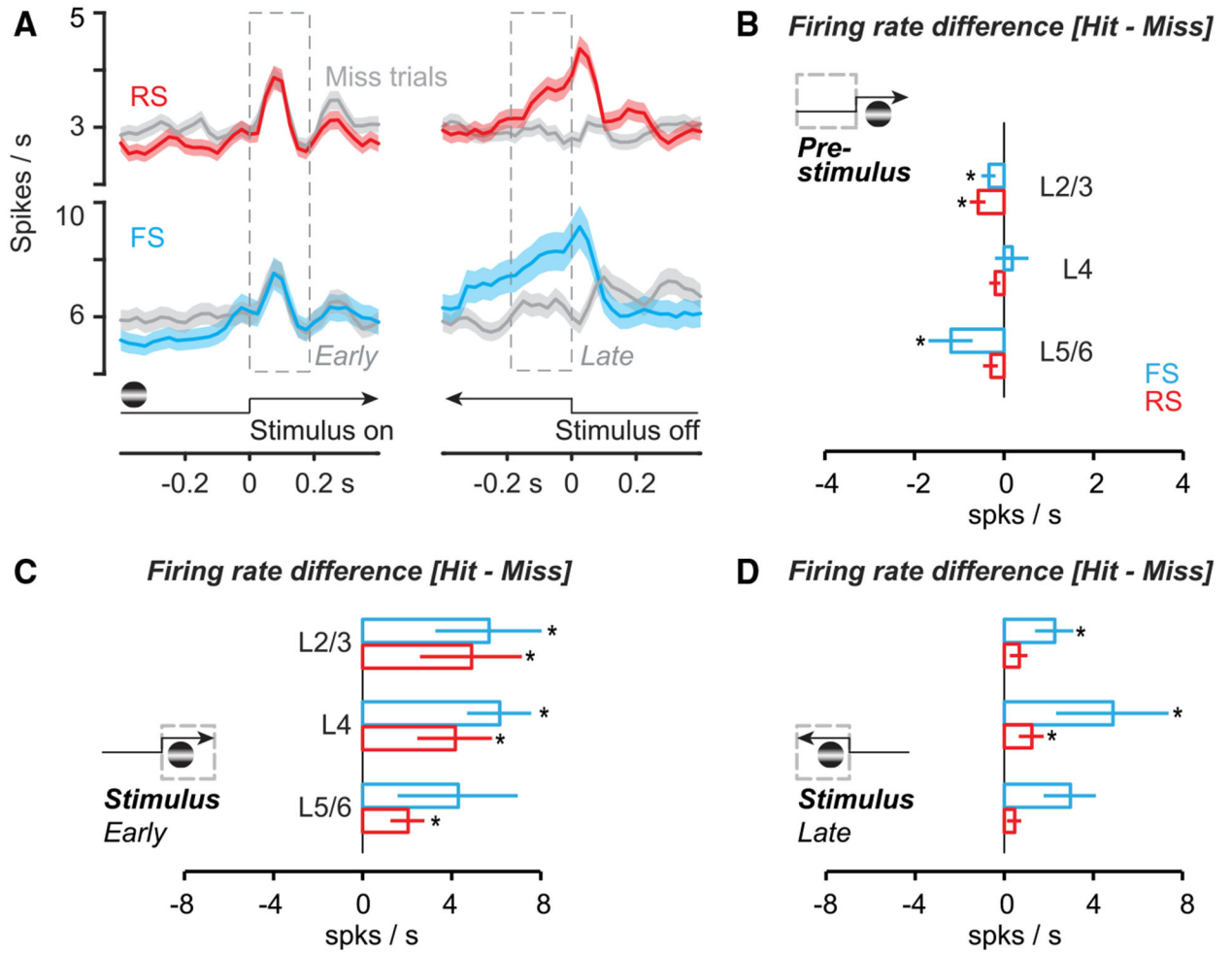


Figure 3. Cortical States with Low Spontaneous Activity Promote Stimulus Detection

(A) Left: regular-spiking (RS) ($n = 172$) and fast-spiking (FS) ($n = 52$; Figure S3) neurons in monocular V1 during monocular detection (Hit trials, colored; Miss trials, gray). Spikes binned at 25 ms, smoothed ± 1 bin. Mean \pm SEM, aligned to stimulus onset. Same experiments as Figure 2. Right: aligned either to first lick (Hit trials) or stimulus offset (Miss trials). See Figure S5 for alignment of Hit trials to stimulus offset. (B) Firing rate difference (Hit minus Miss) before stimulus onset for RS and FS neurons across layers. RS cells fired significantly less before Hit trials in L2/3 (-0.6 ± 0.2 spikes/s; $p < 0.01$), but not in L4 (-0.2 ± 0.1 ; $p = 0.09$) or L5/6 (-0.3 ± 0.2 ; $p = 0.05$). Mean \pm SEM, cell-by-cell paired signed rank for all (see Figure S7). FS cells also fired significantly less in L2/3 before Hit trials (-0.3 ± 0.2 spikes/s; $p = 0.04$) and L5/6 (-1.2 ± 0.5 ; $p = 0.03$), but not in L4 ($+0.2 \pm 0.4$; $p = 0.7$). (C) Similar to (B), for firing rate difference in early stimulus period (0–0.2 s after stimulus onset). RS neurons across all layers fired significantly more during Hit trials (L2/3, $+4.9 \pm 2.3$; L4, $+4.1 \pm 1.7$; L5/6, $+2.0 \pm 0.8$; $p < 0.01$ for all; Figure S5). FS neurons also fired significantly more in L2/3 (5.6 ± 2.4 ; $p < 0.01$) and L4 (6.1 ± 1.4 ; $p < 0.01$), but not in L5/6 (4.3 ± 2.7 ; $p = 0.4$). (D) Similar to (B), for firing rate difference in late stimulus period (–0.2 s to stimulus offset on Misses, or first lick on Hits). In L4, both RS (1.2 ± 0.6 ; $p < 0.01$) and FS (4.9 ± 2.5 ; $p = 0.02$) neurons fired significantly more on Hit trials, as did FS neurons in

L2/3 (2.2 ± 0.9 ; $p < 0.01$). See Figure S5 for firing rate differences relative to pre-stimulus baseline.

Author Manuscript

Author Manuscript

Author Manuscript

Author Manuscript

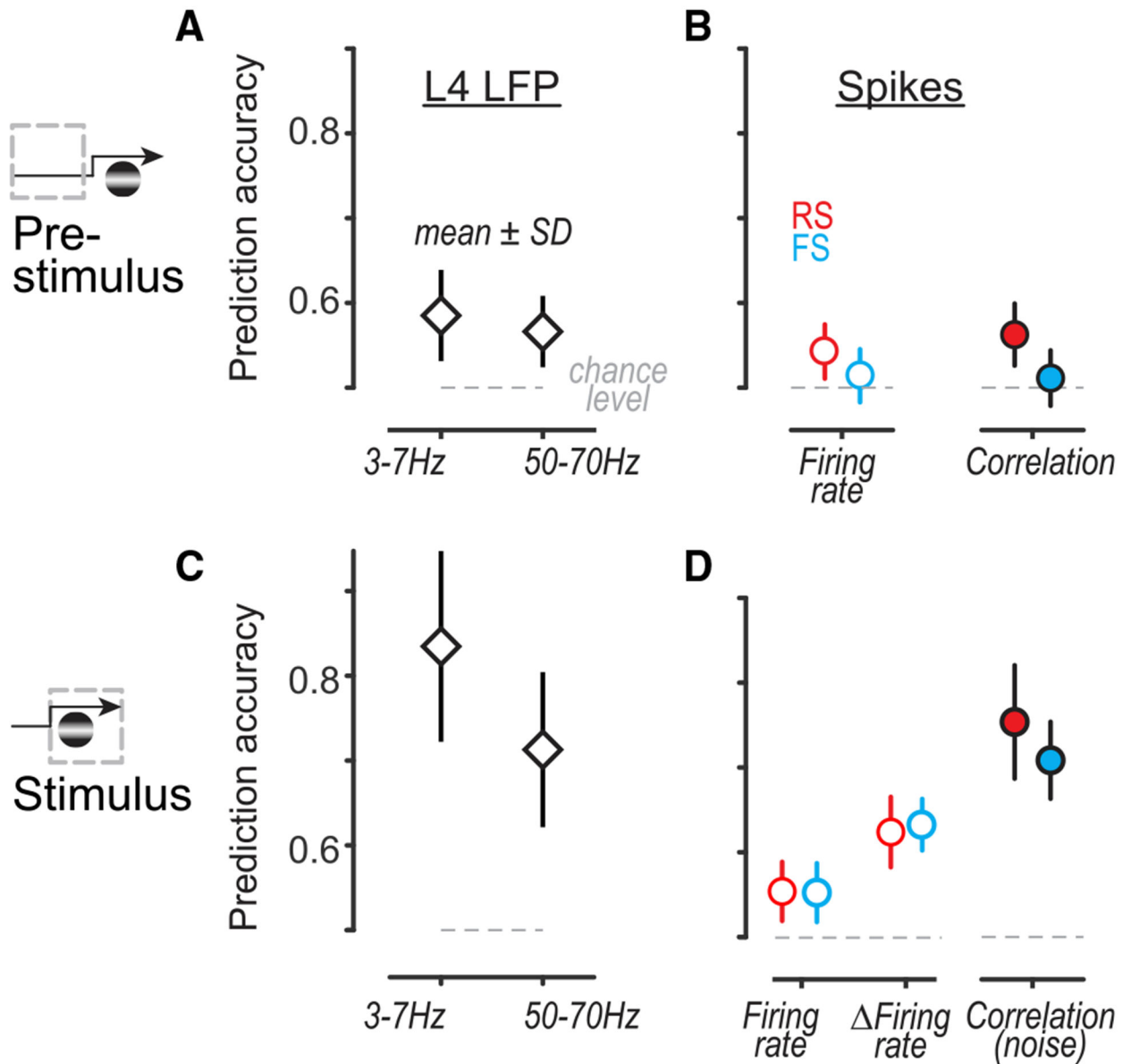


Figure 4. RS Activity and L4 LFP Oscillations Predict Single-Trial Behavior

(A) Pre-stimulus LFP power in L4 predicted single-trial behavioral outcome significantly better than chance (L4 3- to 7-Hz residual power, $59 \pm 5\%$; L4 LFP narrowband gamma 50- to 70-Hz residual power, $57 \pm 4\%$; mean \pm SD; $p < 0.01$, sign test for all). Prediction quality not significantly different between frequency bands ($p = 0.8$; Kruskal-Wallis nonparametric ANOVA with Tukey correction for multiple comparisons throughout). For cross-validated linear classifier, see STAR Methods. (B) Pre-stimulus RS firing rates (left, $54 \pm 4\%$) and RS \times RS pairwise correlations (right, $56 \pm 4\%$) predicted single-trial behavioral outcome significantly better than chance ($p < 0.01$, sign test), as did FS firing rates ($51 \pm 4\%$) and FS \times FS correlations ($51 \pm 4\%$; $p = 0.01$ and $p = 0.02$). No significant difference between prediction quality from RS rates or correlations ($p = 0.1$). RS and FS neurons aggregated across layers; see Figure S6 for laminar predictions. (C) Same as (A), for predictions from

LFP power during stimulus. Stimulus-evoked L4 3- to 7-Hz power predicted single trials with $84 \pm 11\%$ accuracy, while suppression of narrowband gamma 50- to 70-Hz power predicted with $71 \pm 10\%$ accuracy. Prediction quality from L4 3- to 7-Hz power was significantly better than that from narrowband gamma power ($p < 0.01$, nonparametric ANOVA, multiple comparisons). (D) Same as (B), for firing rates and correlations during stimulus. Both RS and FS firing rates predicted single trials better than chance (RS, $55 \pm 4\%$; FS, $55 \pm 4\%$). Evoked firing rates relative to pre-stimulus baseline (Firing rate) predicted significantly better than raw firing rates (RS, $62 \pm 4\%$; FS, $63 \pm 3\%$; $p < 0.001$ for comparisons to firing rates; aggregated across layers). Pairwise noise correlations during the stimulus predicted behavioral outcome most accurately (RS, $75 \pm 7\%$; FS, $71 \pm 4\%$; $p < 0.001$ for RS and $p = 0.07$ for FS for comparisons to Firing rates; aggregated across layers). For laminar predictions from Firing rates and correlations, see Figure S6.

KEY RESOURCES TABLE

REAGENT or RESOURCE	SOURCE	IDENTIFIER
Chemicals, Peptides, and Recombinant Proteins		
Muscimol (Figure S1)	Sigma-Aldrich	M1523
Experimental Models: Organisms/Strains		
Mouse C57BL6 (all Main figures)	Jackson Laboratory	IMSR_JAX:000664
Mouse PV-cre (Figure S1)	Jackson Laboratory	IMSR_JAX:017320
Mouse Ai-32-ChR2 (Figure S1)	Jackson Laboratory	IMSR_JAX:024109
Software and Algorithms		
MATLAB	Mathworks, Inc.	https://www.mathworks.com/
KlusterSuite	Rossant et al., 2016	https://kluster.readthedocs.io/en/latest/

Author Manuscript

Author Manuscript

Author Manuscript

Author Manuscript